HHS Public Access

Author manuscript

Int J Hyperthermia. Author manuscript; available in PMC 2019 November 01.

Published in final edited form as:

Int J Hyperthermia. 2018 November ; 34(7): 934–942. doi:10.1080/02656736.2018.1462535.

Radiofrequency ablation (RFA) induced systemic tumor growth can be reduced by suppression of resultant heat shock proteins

Muneeb Ahmed[1], **Gaurav Kumar**[1], **Svetlana Gourevitch**[2], **Tatyana Levchenko**[3], **Eithan Galun**[4], **Vladimir Torchilin**[3], **S. Nahum Goldberg**[1,2,4]

[1]Laboratory for Minimally Invasive Tumor Therapies, Department of Radiology, Beth Israel Deaconess Medical Center/Harvard Medical School, Boston, MA;

[2]Division of Image-guided Therapy and Interventional Oncology, Department of Radiology, Hadassah Hebrew University Medical Center, Jerusalem, Israel;

[3]Department of Pharmaceutical Sciences and Center for Pharmaceutical Biotechnology and Nanomedicine, Northeastern University, Boston, MA

[4]Department of Gene Therapy, Hadassah Hebrew University Medical Center, Jerusalem, Israel

Abstract

PURPOSE: To determine the role of hepatic RFA heating parameters and their activation of heat shock proteins (HSPs) in modulating distant tumor growth.

METHODS: First, to study effects of RFA dose on distant tumor growth, rats with subcutaneous R3230 adenocarcinoma(10±1mm) were assigned to 3 different hepatic RF doses(60°Cx10min, 70°Cx5min, or 90°Cx2min) that induced identical sized ablation or sham(n=6/arm). Post-RFA tumor growth rates, cellular proliferation(Ki-67), and microvascular density(MVD) were compared at 7d. Next, the effect of low and high power doses on local HSP70 expression and cellular infiltration(α-SMA+ myofibroblasts and CD68+ macrophages), cytokine(IL-6) and growth factor(HGF and VEGF) expression was assessed. Finally, 60°Cx10min and 90°Cx2min RFA were combined with anti-HSP micellar quercetin(MicQ, 2mg/ml). A total of 150 animals were used.

RESULTS: Lower RF heating(70°Cx10min) resulted in larger distant tumors at 7d(19.2±0.8mm for both) while higher RF heating(90°Cx2) led to less distant tumor growth(16.7±1.5mm, $p<0.01$ for both), though increased over sham(13.5±0.5mm, $p<0.01$). Ki-67 and MVD correlated with tumor growth($p<0.01$ for all). Additionally, lower dose 60°Cx10min hepatic RFA had more periablational HSP70 compared to 90°Cx2min(rim: 1,106±163μm vs. 360±18μm, $p<0.001$), with similar trends for periablational α-SMA, CD68, and CDC47($p<0.01$ for all). Anti-HSP70 MicQ blocked distant tumor growth for lower dose(60°Cx10: RF/MicQ 14.6±0.4mm vs. RF alone: 18.1±0.4mm, $p<0.01$) and higher dose RFA(90°Cx2min: RF/MicQ 14.6±0.5mm vs. RF alone: 16.4±0.7mm,$p<0.01$).

Corresponding Author (and address for reprint requests): Muneeb Ahmed, M.D., Department of Radiology, WCC 308-B, Beth Israel Deaconess Medical Center, 1 Deaconess Road, Boston, MA02215, Phone: 617-754-2674, Fax: 617-754-2545, mahmed@bidmc.harvard.edu.

All other authors have no conflicts to report.

CONCLUSION: Hepatic RF heating parameters alters periablational HSP70, which can influence and stimulate distant tumor growth. Modulation of RF heating parameters alone or in combination with adjuvant HSP inhibition can reduce unwanted, off-target systemic tumorigenic effects.

INTRODUCTION

Thermal tumor ablation using either radiofrequency (RF) or microwave (MW) energy is now used commonly in clinical practice for both first- and second-line treatment of primary and secondary liver cancers (1, 2). While substantial improvements in local control and overall survival have been documented for the majority of patients so treated, there is ever increasing awareness that locally *'*curative*'* ablation may have unintended systemic side effects, including stimulation of tumor cells present remote from the site of ablation in some cases (3–5). Indeed, clinical studies have reported up to a 25–39% higher incidence of distant intrahepatic new tumor incidence in patients treated with ablation for either hepatocellular carcinoma or colorectal liver metastases compared to surgical resection (5–8). Thus, strategies to identify and inhibit the potential causes responsible for such *'*off-target*'* pro-oncogenic effects will likely be crucial to improving overall clinical outcomes of thermal ablation.

Recent studies have linked several contributing factors to such off-target effects of hepatic RF thermal ablation (9–11). Experimental studies have identified a host of factors that are upregulated following tumor ablation both within the liver and at distant sites of extrahepatic tumor. These include not only elevation of heat shock proteins (12), but also periablational inflammatory cell recruitment (13), increased local and serologic levels of markers of inflammation (including interleukin-6 (14) and cyclooxygenase receptor activation (15)), growth factor production (particularly the hepatocyte growth factor/c-Met receptor and PI3K/Akt pathways (9, 16)), and expression of pro-angiogenic factors (VEGF and HIF-1α) (11, 17). Many of these pathways have known links to tumor growth, metastasis, and tumor cell invasion, with several recent clinical studies specifically linking elevated IL-6 and HGF blood levels after hepatic RF ablation to poor clinical outcomes (16). Moreover, a large proportion of these tissue reactions occur predominantly in normal non-tumorous liver surrounding the ablation zone that has received a sub-lethal hyperthermic heating dose (i.e. the very region of the ablative margin of normal liver required in all cases of successful ablation) (9, 14).

The extent to which this post-ablation tumorigenic phenomenon is related to the type and dose of energy used is currently only partially answered. In a recent study using hepatic MW ablation, the use of high energy, shorter ablation times to create an identical-sized ablation zone obtained using a lower energy, longer ablation time protocol not only reduced local periablational inflammatory cell recruitment and heat shock protein 70 (HSP70) expression, but also reduced distant subcutaneous tumor growth as well (18). Additionally, although it has been previously demonstrated that the dose of RF ablation can substantially alter HSP expression surrounding similar sized ablation zones (19), whether such changes in dose can affect the extent of RF-induced tumorigenesis and any potential relationship to HSP production is currently unknown. Nevertheless, given the known association between heat shock proteins and cancer cell survival, including activation of some pathways implicated in

ablation-induced tumor stimulation (such as HIF-1a and VEGF), we hypothesized that reducing periablational non-lethal hyperthermic effects via specific HSP inhibitors may offer an additional way to reduce off-target ablation-induced tumor stimulation (20). Accordingly, here, we study the effect of hepatic RF ablation thermal dose on downstream distant subcutaneous tumor growth attempting to correlate this phenomenon with periablational HSP70 expression, inflammation, and cytokine expression in a well-established rodent model. Thereafter, we studied the potential benefit of local periablational HSP suppression with adjuvant micellar quercetin (Mic-Qu) when combined with different RF thermal doses to determine the role of HSP on off-target effects of hepatic ablation.

MATERIALS AND METHODS

Overview of experimental design:

Approval of the Institutional Animal Care and Use Committee was obtained for all studies. Our study was performed in four parts, for which a total of 150 female Fisher 344 (F344) rats were used. Initially, three standardized thermal ablation protocols were compared ('lower power, longer duration' RFA with power titrated to a tip temperature of 60°C applied for 10 min, 'medium power, intermediate duration' RFA with tip temperatures of 70°C for 5 min, and 'higher power, shorter duration' RFA at 90°C for 2 min, all in normal liver to simulate the standard clinical endpoint of ablating a margin of normal liver (21, 22). All three of these doses have previously been shown to result in similarly-sized ablation zones (6.1 ± 0.1 mm) in the models studied here (19). A control arm of sham treatment with probe placement without applicator activation/ablation was also introduced. First, the effects of three hepatic ablation protocols on distant subcutaneous tumor growth were assessed. R3230 breast adenocarcinoma tumors were implanted 'in situ' in the mammary fat pad of animals, and tumors were measured daily until they reached a mean diameter of 10–11 mm, at which point they were randomly assigned to one of 4 arms (3 doses and 1 sham procedure arm x n=6/arm = 24 animals). The primary outcome was the evaluation of tumor growth (tumor size and growth curve analysis comparisons) with secondary immunohistochemical outcomes of tumor proliferation (Ki-67) and microvascular density (MVD, with CD34 staining). Based on these results, in which the 'lower power' and 'medium power' arms had similar effects on distant tumor growth, all subsequent steps compared 'low power, longer duration' 60°C x 10 min to 'higher power, shorter duration' 90°C x 2 min. Next, for the low and high power hepatic RF ablation protocols (and control animals), periablational heat shock protein-70 (HSP70) expression were compared 24h after treatment (3 arms x n=6/arm = 18 animals). The effects of hepatic RF ablation protocol on cytokine (interleukin-6) and growth factor (HGF and VEGF) expression were compared (3 arms x n=6/arm x 2 time points = 36 animals). IL-6 was measured 6hr after ablation in both periablational tissue and serum, while HGF and VEGF were measured 72h after ablation in periablational tissue, serum, and distant subcutaneous R3230 tumor, as these represent peak expression times after hepatic RF ablation (9, 14). Additionally, the extent of alpha-smooth muscle actin-positive (α-SMA) hepatic stellate cell / activated myofibroblasts and macrophages in the periablational border zone was evaluated at 72hr. Finally, in an additional group of 72 animals, micellar quercetin, a known HSP70 inhibitor (23), was administered as an adjuvant to low power, long duration and high power, short duration hepatic RFA protocols (with

sham/micellar quercetin as a control) to assess its effects on periablational HSP70 (at 24h), cellular recruitment (at 24h and 72h), post-ablation IL-6 (at 6h) and growth factor production (at 72h), and distant tumor growth (at 7d) (3 additional treatment arms n=6/arm x 4 time points).

RF Application:

Conventional monopolar RFA was applied by using a 500-kHz RFA generator (model CC-1; Radionics, Burlington, MA), as has been previously described (24). Initially, the 1-cm tip of a 21-gauge electrically insulated electrode (SMK electrode; Radionics) was placed at the center of the tumor. For livers, after exposure and visualization of the right lobe the probe was inserted in the liver with its long axis parallel to the long axis of the lobe. Complete insertion in the liver was confirmed visually before performing RF ablation. For each thermal dose, RF was applied for a predetermined number of minutes with the generator output titrated to maintain a designated tip temperature. To complete the RF circuit, the animal's back was shaved and water-soluble ultrasound gel was applied to ensure proper conduction with the metallic grounding pad (Radionics).

Animal Models:

For all experiments and procedures, anesthesia was induced with intraperitoneal (IP) injection of a mixture of ketamine (50 mg/kg, Ketaject; Phoenix Pharmaceutical, St. Joseph, MO) and xylazine (5 mg/kg, Bayer, Shawnee Mission, KS), and post-procedure analgesia was provided with standardized subcutaneous buprenorphine (0.3mg/kg). Animals were sacrificed with an overdose of carbon dioxide (SMARTBOX™ CO2 Chamber System, EZ systems, Palmer, PA). In the first part of our study, Fisher 344 rats without tumors were used. In the second and third phase, experiments were performed in a well-characterized R3230 mammary adenocarcinoma model in which hepatic RF ablation leads to distant tumor growth (9, 14). Cell lines were implanted subcutaneously in the mammary fat pad of female F344 rats (150±20g; 14–16 weeks old, Charles River, Wilmington, MA). Tumor implantation, evaluation, and preparation techniques were performed as previously described (9). Briefly, one tumor was implanted into each animal by slowly injecting 0.3–0.4 mL of tumor suspension into the mammary fat pad of each animal via an 18-guage needle.

Preparation and administration of adjuvant IV Quercetin:

Quercetin-loaded micelles were prepared by lipid film hydration method as previously described (23, 25). Briefly, 0.6 mg of quercetin (1 mg/mL solution in methanol) was added to polyethylene glycol-lphosphatidylethanolamine (PEG2000-PE) solutions in chloroform, and a lipid film was formed in a round-bottomed flask by solvent removal on a rotary evaporator. The lipid film was then rehydrated with 1mL of phosphate buffered saline, pH 7.4 to obtain final lipid concentration 5 mM. The sample was vortexed for 15 min at room temperature and the unincorporated quercetin was removed by filtration of the micelle suspension with 0.2μm membrane filters. The micellar loading efficiency of quercetin was 100% (as noted above, 0.6mg of quercetin was loaded in each ml). The micelle size was 17.0±2.1 nm and zeta-potential was −21.7±4.3 mV. Mic-Qu was administered via tail vein intravenous injection 15 min post RFA. This timing of administration was selected based upon prior studies combining RFA with nano-drugs demonstrating maximum intratumoral

drug accumulation with this regimen (24). Agents were stored at 4°C in light-proof containers and loaded exactly at time of administration to avoid precipitation.

Pathologic evaluation:

Animals were sacrificed and tissue harvested. Livers and tumors were sectioned perpendicularly to the direction of electrode insertion. The relevant portion of the liver or one half of the tumor containing the central section of tumor was fixed in 10% formalin overnight at 4°C, embedded in paraffin, and sectioned at a thickness of 5 μm. Tissues were stained with hematoxylin-eosin for histopathologic assessment.

Tumor growth measurements:

For both RF alone and RF / micellar quercetin studies, tumors were measured in a longitudinal and transverse diameter using mechanical calipers and an average diameter was calculated. Measurements were taken every 1–2 days until the tumors reached 6–7 mm, at which point they were measured daily. Once tumors reached the target mean diameter of 10 mm they were randomly allocated to treatment arms. Following ablation or sham treatment, measurements were obtained daily for 7 days.

Quantification of IL-6, HGF, and VEGF:

Serum and tissue samples (periablational and/or distant tumor, where specified) were harvested at 6hr after treatment for IL-6 and 72hr after treatment for VEGF and HGF, as previous studies have demonstrated peak concentrations at these times (10, 14, 26). For liver samples, tissues were specifically harvested from the periablational rim. Samples were assayed for IL-6 (rat/R6000B Quantikine kit, R&D Systems), HGF (rat/MHG00 Quantikine kit, R&D Systems Inc. Minneapolis, MN) and VEGF (rat/RRV00 Quantikine kit, R&D Systems) using an enzyme-linked immunosorbent assay (ELISA) kit according to the manufacturer's instructions. Flash-frozen liver and tumor tissue was homogenized in a cold lysis buffer (Cell Signaling Technology Inc., Beverly, MA) consisting of 0.1% proteinase inhibitor (Sigma-Aldrich). The homogenates were then centrifuged at 14,000 rpm for 20 minutes at 4°C, and the total protein concentrations were determined using a bichinchoninic acid method (BCA) (Sigma-Aldrich). IL-6, VEGF, and HGF values were then normalized to protein concentration. Undiluted serum was used. All samples were measured in duplicate, and the average value was recorded (9).

Immunohistochemistry:

Histopathologic evaluation was performed on tissues from the primary site of liver ablation, from untreated liver tissue from the contralateral lobe where specified, and from distant subcutaneous tumors. All samples were fixed in 10% formalin for 48hr at 4°C, embedded in paraffin blocks, and sectioned at a thickness of 5 μm. Specimen slides were imaged and analyzed using a Micromaster I microscope (Fisher Scientific, Pittsburgh, PA) and Micron Imaging Software (Westover Scientific Inc., Mill Greek, WA). Four random high power fields were analyzed for a minimum of 3 specimens per parameter. Immunohistochemical staining and quantification for macrophages (CD68, # positive cells per hpf) and heat shock protein 70 (HSP70, rim thickness) were performed to assess ablation-induced tissue

responses, as has been described previously (13, 14). Based on prior work demonstrating optimal detection with specific markers, IHC protocols were performed to assess proliferative indices. CDC47 antibody was used to assess hepatocyte proliferation and liver regeneration (47DC141, Diagnostic BioSystems, Pleasanton, CA), Ki-67 antibody to assess distant tumor cellular proliferation (Ab16667, Abcam, Cambridge, MA), and CD34 to assess distant tumor microvascular density (AF4117, R & D Systems). For Ki-67 and CDC47, % cell positivity (ratio of positive cells to the sum of positive and negative cells) was calculated for each field and averaged for each sample. Quantification was performed for CD34 by counting the number of cells positive per high-powered field (hpf).

Statistical analysis:

All data were expressed as mean plus or minus standard deviation. Selected mean tumor sizes (day 0 and at the time of sacrifice), and immunohistochemical quantification were compared using analysis of variance (ANOVA) with testing including a post-treatment interaction term. Additional post-hoc analysis was performed with a two-sample, two-tailed Student's T-test, if and only if, the analysis of variance achieved statistical significance. A P value of less than 0.05 was considered significant. Tumor growth curves before and after treatment were analyzed using linear regression analysis models to determine the slope of the pre- and post-treatment growth curve on a per-tumor basis. From these data, mean post-treatment growth curve slopes plus or minus SD were then calculated and compared using ANOVA and paired, two-tailed T-tests.

RESULTS

Effect of hepatic RF ablation dose on distant R3230 tumor growth.

Pre-operative tumor sizes and growth rates were equivalent at 9.8±0.8 mm and 0.58±0.03 mm/day, respectively (Table 1). Hepatic ablation with low (60°Cx10min), medium (70°C x5min), and high (90°C x2min) temperature increased the growth of the distant untreated subcutaneous tumor, resulting in significantly larger tumors at 7d compared to sham (60°Cx10min: 18.1±0.4mm, 70°C x5min: 19.2±0.8mm, 90°Cx2min: 16.4±0.7mm vs. sham: 13.5±0.5mm, $p<0.05$ for all comparisons, Figure 1). Although greater than sham treatment ($p=0.01$), tumor growth (16.4±0.7mm) was significantly lower for the high temperature, short duration (90°Cx2min) protocol than both lower temperatures with longer heating times (i.e. 60°Cx10min and 70°C x5min RF protocols) ($p<0.05$, for all comparisons), (Figure 1, Table 1). Additionally, all RFA protocols increased tumor growth rates after treatment (pre-ablation growth slope: 60°Cx10min: 0.59±0.09 mm/d, 70°Cx5min: 0.58±0.09 mm/d, 90°Cx2min 0.60±0.09 mm/d; vs. post-ablation slope: 60°Cx10min: 1.22±0.13 mm/d, 70°Cx5min: 1.26±0.07 mm/d, 90°Cx2min: 0.85±0.08 mm/d, $p<0.01$ all three comparisons), while no significant difference was observed for sham untreated liver (pre-ablation growth slope-sham: 0.54±0.03 mm/d; post-ablation slope sham: 0.47±0.06 mm/d, $p=0.48$).

In the distant R3230 tumors, increased cellular proliferation (Ki-67, % cell positivity) was greater for low and medium power RFA (60°Cx10min: 58.4±1.0%, 70°Cx5min: 63.6±4.3%cells/hpf, $p=0.55$), compared to high power RFA (90°C x2min: 43.6±1.6%, $p<0.001$ all comparisons), all of which had greater distant tumor proliferation at 7d post-

treatment compared to sham-treated distant tumors (19.4±1.2%, p=<0.01 for all comparisons). Likewise, increases in distant tumor microvascular density (CD34 staining) followed a similar trend, with significant increases observed for low and medium power RFA (22.6±3.1 vessels positive per hpf) compared to high power RFA (16.7±1.5, p<0.01), all greater than sham treatment (13.8±0.3, p<0.05) (Table 1).

Periablational HSP70 and inflammatory cell recruitment correlates with hepatic RFA dose.

Hepatic RFA using both low and high power applications resulted in increased HSP70 expression within the periablational rim (rim thickness: 60°Cx10min: 1106±16um vs.90°C x2min: 360±18um; % cell positivity: 60°Cx10min: 21.0±2.6% vs.90°C x2min: 14.2±1.5%) compared to sham treatment where no HSP70 was detected at the site of needle insertion. Yet, low power settings resulted in greater amounts of HSP70 expression compared to high power setting (p<0.05 for all comparisons).

Lower power RFA (60°Cx10min: 45.4±21.7 cells/hpf) increased periablational a-SMA+ myofibroblasts at 3d over both sham treatment (10.7±2.1 cells/hpf, p=0.01) and higher power RFA (90°Cx2min 19.0±9.9 cells/hpf, p<0.01). No difference was observed in periablational myofibroblasts between higher power RFA and sham treatment. However, both thermal doses increased periablational macrophage recruitment at 7d compared to sham treatment (10.5±4.9 cells/hpf), with 37.8±17.2 cells/hpf and 40.9±18.0 cells/hpf observed at 60°Cx10min and (90°C x2min, respectively (p<0.05 for both comparisons). No difference was observed in macrophage recruitment between low and high thermal dose RFA. Yet, 60°Cx10min RFA demonstrated lower levels of periablational CDC47-positive cell proliferation (10.7±4.6 cells/hpf) compared to higher power RFA (90°C x2min: 4.3±1.2 cells/hpf, p<0.01).

Cytokine and growth factor elevation following hepatic ablation:

Low and high-dose hepatic RFA both increased local periablational liver IL-6 levels (60°Cx10min: 2956±265 pg/ml, 90°Cx2min: 2486±72 pg/ml) compared to sham treatment (2189±106 pg/ml, p<0.01 for all comparisons)(Table 2). Yet, low dose ablation resulted in greater local IL-6 expression than high-dose RFA (p<0.01). A similar trend was observed for serum IL-6 expression, with increases observed at 6h post-ablation for RFA compared to sham treatment (60°Cx10min: 452±8 pg/ml 90°C x2min: 348±17 pg/ml, sham: 264±7 pg/ml, p<0.01 for all comparisons, Table 2), which was greater for low dose RFA (p<0.01 vs. high dose).

Hepatic RFA, increased periablational HGF levels compared to sham at 72h after treatment regardless of thermal dose (60°Cx10min: 33619±1110 pg/ml, 90°Cx2min: 25453±752 pg/ml, sham: 21758±961 pg/ml, p<0.01 for all comparisons, Table 2), once again greater for low dose compared to high dose RFA (p<0.01). Similarly, serum HGF levels were increased at 72h post-ablation for both RFA doses compared to sham treatment (60°Cx10min: 3987±47 pg/ml, 90°C x2min: 3537±202 pg/ml, sham: 2851±208 pg/ml, p<0.01 for all comparisons, Table 2), again greatest for low dose RFA (p<0.01).

Finally, VEGF levels at 72h after treatment were increased for both ablation arms compared to sham treatment (sham: 7536±127, 60°Cx10min: 13036±1214 pg/ml, 90°Cx2min:

8925±464 pg/ml, p<0.01 for all comparisons, Table 2), also greatest for low dose hepatic RFA.

Effect of adjuvant quercetin on periablational HSP70 expression, local and serum cytokine expression, and distant tumor growth.

Subcutaneous tumor growth rates for all pre-treatment arms (adjuvant MQ with sham, low dose 60°Cx10min, and high dose 90°Cx2min) was statistically identical (mean growth rate 1.01±0.23mm/d). Single-dose adjuvant MQ reduced the tumor size at 7d to baseline control tumor levels for both the low and high RFA power settings (60°Cx10min/MQ 14.6±0.4mm and 90°Cx2min/MQ 14.6±0.5 mm vs. sham treatment/MQ 14.1±0.6 mm, p=NS, Table 1, Figure 2).

Adjuvant MQ combined with hepatic RFA reduced HSP70 expression in the periablational rim for low- and high-dose RFA compared to hepatic RFA alone, for both rim thickness (60°Cx10min 1106±16 um, 60°Cx10min/MQ 311±18 um; 90°Cx2min 360±18; 90°Cx2min/MQ 129±3um, p<0.05 for both comparisons) and % cell positivity (60°Cx10min 21.0±2.6%, 60°Cx10min/MQ 11.7±2.2%; 90°Cx2min 14.2±1.5%, 90°Cx2min/MQ 11.5±1.9%, p<0.05 for both comparisons, Figure 3).

Adjuvant micellar quercetin also reduced IL-6 production back to baseline levels for both high-dose/MQ and low-dose/MQ hepatic RFA compared to sham/MQ in the periablational margin (60°Cx10min/MQ 2903±108 pg/ml, 90°Cx2min/MQ 2503±60 pg/ml vs. sham/MQ 2167±134 pg/ml, p=NS). By contrast, serum IL-6 levels after hepatic ablation plus MQ remained higher than sham (60°Cx10min/MQ 442±18 pg/ml, 90°Cx2min/MQ 359±19 pg/ml, sham/QM 262±9 pg/ml, p<0.05 for both comparisons). Adjuvant MQ not only reduced HGF levels after high- and low-dose hepatic RFA compared to baseline levels of sham/MQ in the periablational rim (60°Cx10min/MQ 22092±507 pg/ml, 90°Cx2min/MQ 21897±1329 pg/ml, sham/MQ 22175±220 pg/ml, p<0.05 for both comparisons), but also in serum (60°Cx10min/MQ 3987±47 pg/ml, 90°Cx2min/MQ 3537±202 pg/ml vs. sham/MQ 2884±317 pg/ml, p=NS). Finally, VEGF levels after ablation combined with adjuvant MQ were still elevated compared to sham/MQ treatment, but lower than low- and high-dose RFA alone (60°Cx10min/MQ 9528±821 pg/ml, 90°Cx2min/MQ 8036±699 pg/ml vs. sham/MQ 7703±293 pg/ml, p<0.05 comparisons).

DISCUSSION

Based on both clinical and experimental studies, there has been significant recent interest in the secondary systemic side effects of image-guided tumor ablative therapies, and in particular, in the potential stimulation of distant tumor separate from the ablation zone (3, 4, 9, 10). Several studies have linked these pro-oncogenic effects to cytokine and growth factor production in the periablational rim of tissue exposed to non-lethal partial heating, along with periablational inflammation and cellular recruitment to the ablation zone (9, 10, 13, 14). Flere, we investigate the role of tissue heat injury, through heat shock expression, on driving post-hepatic RF ablation -induced systemic tumorigenic effects.

In this study, we identify an additional, potentially novel role of hepatic RFA-induced periablational HSP70 expression in driving pro-oncogenic distant tumor stimulation. Recent work has identified a key mechanistic pathway, IL-6-HGF/c-Met-STAT3-VEGF axis, as a central driver of systemic pro-oncogenic off-target effects of RF ablation (9, 14, 27). Yet, our findings demonstrate that periablational HSP70, which to date has no known established links to IL-6 or HGF/c-Met, can also be implicated in the stimulation of distant tumor growth. This introduces the prospect that parallel 'escape' pathways may also be contributing to tumor stimulatory effects of hepatic ablation. Heat shock proteins have known links to inflammation, hypoxia (HIF-1α), and such pro-tumor pathways that regulate cellular stress response and metabolism (28, 29). Heat cell stress has been linked to changes related to more aggressive tumor cell biology when residual cells remain (30), and use of anti-HSP agents have been previously used to increase local periablational cytotoxicity in partially heat-injured cells (23). Accordingly, HSP70 represents a particularly appealing multi-faceted target that now may be even more potentially useful as additional separate target to block RFA-mediated tumor stimulation.

We also demonstrate that variable doses of hepatic RF ablation, despite inducing similar ablation zones, can have a substantial impact upon tumor growth in distant subcutaneous tumors. This finding is consistent with a recent study demonstrating that different heating paradigms for hepatic microwave ablation also resulted in differential distant tumor growth rates (18). Similar to MW ablation, we note that a high temperature / shorter duration paradigm offers the best approach to limited off-target pro-oncogenic effects after hepatic RF ablation. Furthermore, secondary tissue reactions such as periablational and serum IL-6 and HGF expression, which are key elements in a mechanistic pathway that are directly linked to distant tumor growth, also demonstrated a 'dose-dependent effect' with RFA heating with concomitant following trend in distant tumor growth. This provides additional evidence that modulation of the ablation administration protocol when clinically feasible could potentially be beneficial in minimizing (though not fully eliminating) periablational inflammation and distant tumorigenic effects. Thus, ablation paradigm development that has often emphasized a 'hotter and faster equals better' approach for improving throughput may provide other physiologic benefits. Regardless, greater optimization of existing platforms and protocols to account for secondary tissue reactions beyond the ablative margin is likely warranted. This extends to many types of ablation as studies have also demonstrated that even traditionally non-thermal ablative modalities such as irreversible electroporation can also incite key tissue reactions and/or stimulate distant tumor growth (31, 32).

Prior studies have demonstrated that the tissue reactions occurring in the periablational rim, including both local reactions such as HSP70 and HIF-1α, and distant off-target tumorigenic effects mediated by HGF/c-Met and VEGF, vary based on thermal ablation heating technique (18, 19). Likewise, in this study, we noted that heat shock protein expression in the periablational rim also correlated with variable hepatic RF ablation, with greater expression occurring for lower power / longer heating 'low-dose' settings. Based upon this, we combined hepatic RFA with micellar quercetin, a nanodrug that can be combined with ablation to suppress periablational heat shock protein expression and has been used to increase the size of the local ablation zone (23). We observed that a single-dose of adjuvant micellar quercetin administered with hepatic RF ablation blocked off-target distant systemic

tumorigenic effects and suppressed distant subcutaneous tumor growth rates back to baseline levels. While nanodrugs loaded with anti-IL6 siRNA have been previously used to block off-target tumor stimulation after hepatic RFA, we note that the anti-HSP70 agent micellar quercetin has the potential for a dual role to increase local ablative cytotoxicity and ablation zone size while simultaneously blocking unwanted off-target pro-tumor effects. Regardless, continued optimization and development of nanodrugs that can target multiple mechanisms or through uses in theranostics after ablation, will likely be of great utility in future studies. Conversely, nanodrug delivery is also influenced by variable tissue heating and extent / width of the periablational rim exposed to partial heating. Indeed, prior studies have demonstrated that micellar forms of quercetin achieved better delivery and were more effective in modulating periablational hypoxia and HSP expression than standard liposomes (33). Accordingly, careful study will be required to successfully balance construction of agents to achieve maximal targeted delivery even while ablation techniques are modified to reduce the extent of periablational tissue that is receptive to nanodrug deposition.

There are several limitations in our study. We readily acknowledge that full quantitative dose-response studies defining the precise relationship between HSP production and tumor growth are currently lacking. Accordingly, it is still unknown as to whether these are stochiastic or true dose dependent effects. Additionally, all the ablations in our study were performed in only one tissue type, normal liver (as this closely simulates the clinical practice of achieving an ablative margin), using one tumor model, subcutaneous ‘in situ’ breast tumors. While similar findings after RFA for other tumor types (de novo HCC in inflammatory cirrhosis in the Mdr2 knockout mouse model) and organs (kidney) have already been reported, additional verification will be required in other settings to understand the true clinical impact of our study’s findings. Furthermore, we acknowledge that ablation energy can be applied with a multitude of energy parameters including durations and intensities. Thus, although the duration and intensities of RFA used in this study accurately reflect a reasonable range of applications in the clinical setting, further study is likely warranted (21, 34). Finally, we acknowledge that our understanding of all of the differences in post-ablation reactions for the wide range of ablation strategies currently available is incomplete and that further mechanistic study is likely warranted. This includes potentially beneficial immunologic effects, including an abscopic effect in some tumor models that can be further enhanced with adjuvant therapies. Therefore, further study of the differences between ablation modalities over a wide range of tumor lines and types (particularly those that demonstrate abscopal effects after RFA) are needed to determine those circumstances where modification of ablation parameters can be used to augment anti-tumor immunity.

In summary, variable hepatic RFA heating using low-dose, longer heating increases periablational HSP70 to a greater extent than higher temperature, faster heating, which can in turn result in greater off-target stimulation of distant tumor. Selective blockade of this HSP70 expression with adjuvant micellar quercetin can successfully suppress ablation-induced distant tumor growth potentially blunting the previously identified IL-6/HGF-cMet/STAT3/VEGF pathway. Continued study of potential additional contributory pathways to off-target effects of tumor ablation with the goal of identification of potential therapeutic targets and modulation of ablation application algorithms is warranted.

Acknowledgments

Sponsored in part by grants from the NIH (5R01CA197081), Israel Science Foundation, and Israel Ministry of Science. SN Goldberg has unrelated sponsored research and consulting from Angiodynamics (Marlborough, MA) and Cosman Instruments (Cambridge, MA).

REFERENCES

1. Gillams A, Goldberg N, Ahmed M, Bale R, Breen D, Callstrom M, et al. Thermal ablation of colorectal liver metastases: a position paper by an international panel of ablation experts, the interventional oncology sans frontieres meeting 2013. European radiology. 2015.
2. Yu J, Yu XL, Han ZY, Cheng ZG, Liu FY, Zhai HY, et al. Percutaneous cooled-probe microwave versus radiofrequency ablation in early-stage hepatocellular carcinoma: a phase III randomised controlled trial. Gut. 2017;66(6):1172–3. [PubMed: 27884919]
3. Kang TW, Kim JM, Rhim H, Lee MW, Kim YS, Lim HK, et al. Small Hepatocellular Carcinoma: Radiofrequency Ablation versus Nonanatomic Resection--Propensity Score Analyses of Long-term Outcomes. Radiology. 2015;275(3):908–19. [PubMed: 25688888]
4. Kang TW, Lim HK, Lee MW, Kim YS, Rhim H, Lee WJ, et al. Aggressive Intrasegmental Recurrence of Hepatocellular Carcinoma after Radiofrequency Ablation: Risk Factors and Clinical Significance. Radiology. 2015;276(1):274–85. [PubMed: 25734550]
5. Tanis E, Nordlinger B, Mauer M, Sorbye H, van Coevorden F, Gruenberger T, et al. Local recurrence rates after radiofrequency ablation or resection of colorectal liver metastases. Analysis of the European Organisation for Research and Treatment of Cancer #40004 and #40983. European journal of cancer. 2014;50(5):912–9. [PubMed: 24411080]
6. Lencioni R, Cioni D, Crocetti L, Franchini C, Pina CD, Lera J, et al. Early-stage hepatocellular carcinoma in patients with cirrhosis: long-term results of percutaneous image-guided radiofrequency ablation. Radiology. 2005;234(3):961–7. [PubMed: 15665226]
7. N'Kontchou G, Mahamoudi A, Aout M, Ganne-Carrie N, Grando V, Coderc E, et al. Radiofrequency ablation of hepatocellular carcinoma: long-term results and prognostic factors in 235 Western patients with cirrhosis. Hepatology. 2009;50(5):1475–83. [PubMed: 19731239]
8. Lee DH, Lee JM, Lee JY, Kim SH, Han JK, Choi BI. Radiofrequency ablation for intrahepatic recurrent hepatocellular carcinoma: long-term results and prognostic factors in 168 patients with cirrhosis. Cardiovascular and interventional radiology. 2014;37(3):705–15. [PubMed: 23912493]
9. Ahmed M, Kumar G, Moussa M, Wang Y, Rozenblum N, Galun E, et al. Hepatic Radiofrequency Ablation-induced Stimulation of Distant Tumor Growth Is Suppressed by c-Met Inhibition. Radiology. 2015:150080.
10. Rozenblum N, Zeira E, Scaiewicz V, Bulvik B, Gourevitch S, Yotvat H, et al. Oncogenesis: An "off-target" effect of radiofrequency ablation. Radiology. 2015:141695.
11. Nijkamp MW, van der Bilt JD, de Bruijn MT, Molenaar IQ, Voest EE, van Diest PJ, et al. Accelerated perinecrotic outgrowth of colorectal liver metastases following radiofrequency ablation is a hypoxia-driven phenomenon. Ann Surg. 2009;249(5):814–23. [PubMed: 19387320]
12. Moussa M, Ahmed M, Kumar G, Sawant RR, Levchenko T, Torchilin VP, et al. Radiofrequency (RF) Ablation: Adjuvant Micellar Quercetin Further Suppresses RF-induced Heat Shock Protein Expression Compared to Liposomal Preparations in a Small Animal Tumor Model Radiological Society of North America Annual Meeting. 2012.
13. Rozenblum N, Zeira E, Bulvik B, Gourevitch S, Yotvat H, Galun E, et al. Radiofrequency ablation: Inflammatory changes in the periablative zone can induce global organ effects, including liver regeneration. Radiology. 2015:141918.
14. Ahmed M, Kumar G, Navarro G, Wang Y, Gourevitch S, Moussa MH, et al. Systemic siRNA Nanoparticle-Based Drugs Combined with Radiofrequency Ablation for Cancer Therapy. PLoS One. 2015;10(7):e0128910. [PubMed: 26154425]
15. Kumar G, Goldberg SN, Wang Y, Velez E, Gourevitch S, Galun E, et al. Hepatic radiofrequency ablation: markedly reduced systemic effects by modulating periablational inflammation via cyclooxygenase-2 inhibition. European radiology. 2016.

16. Hinz S, Tepel J, Roder C, Kalthoff H, Becker T. Profile of serum factors and disseminated tumor cells before and after radiofrequency ablation compared to resection of colorectal liver metastases - a pilot study. Anticancer research. 2015;35(5):2961–7. [PubMed: 25964582]
17. Kong J, Kong J, Pan B, Ke S, Dong S, Li X, et al. Insufficient radiofrequency ablation promotes angiogenesis of residual hepatocellular carcinoma via HIF-1alpha/VEGFA. PLoS One. 2012;7(5):e37266. [PubMed: 22615958]
18. Velez E, Goldberg SN, Kumar G, Wang Y, Gourevitch S, Sosna J, et al. Hepatic Thermal Ablation: Effect of Device and Heating Parameters on Local Tissue Reactions and Distant Tumor Growth. Radiology. 2016;281(3):782–92. [PubMed: 27409564]
19. Moussa M, Goldberg SN, Kumar G, Levchenko T, Torchilin V, Ahmed M. Effect of thermal dose on heat shock protein expression after radio-frequency ablation with and without adjuvant nanoparticle chemotherapies. Int J Hyperthermia. 2016;32(8):829–41. [PubMed: 27600101]
20. Yang W, Ahmed M, Tasawwar B, Levchenko T, Sawant RR, Torchilin V, et al. Combination radiofrequency (RF) ablation and IV liposomal heat shock protein suppression: reduced tumor growth and increased animal endpoint survival in a small animal tumor model. Journal of controlled release : official journal of the Controlled Release Society. 2012;160(2):239–44. [PubMed: 22230341]
21. Ahmed M, Brace CL, Lee FT Jr., Goldberg SN. Principles of and advances in percutaneous ablation. Radiology. 2011;258(2):351–69. [PubMed: 21273519]
22. Wang X, Sofocleous CT, Erinjeri JP, Petre EN, Gonen M, Do KG, et al. Margin size is an independent predictor of local tumor progression after ablation of colon cancer liver metastases. Cardiovascular and interventional radiology. 2013;36(1):166–75. [PubMed: 22535243]
23. Yang W, Ahmed M, Tasawwar B, Levchenko T, Sawant RR, Collins M, et al. Radiofrequency ablation combined with liposomal quercetin to increase tumour destruction by modulation of heat shock protein production in a small animal model. Int J Hyperthermia. 2011;27(6):527–38. [PubMed: 21846189]
24. Ahmed M, Monsky WE, Girnun G, Lukyanov A, D'Ippolito G, Kruskal JB, et al. Radiofrequency thermal ablation sharply increases intratumoral liposomal doxorubicin accumulation and tumor coagulation. Cancer Res. 2003;63(19):6327–33. [PubMed: 14559820]
25. Sawant RR, Sriraman SK, Navarro G, Biswas S, Dalvi RA, Torchilin VP. Polyethyleneimine-lipid conjugate-based pH-sensitive micellar carrier for gene delivery. Biomaterials. 2012;33(15):3942–51. [PubMed: 22365809]
26. D'Ippolito G, Ahmed M, Girnun GD, Stuart KE, Kruskal JB, Halpern EF, et al. Percutaneous tumor ablation: reduced tumor growth with combined radio-frequency ablation and liposomal doxorubicin in a rat breast tumor model. Radiology. 2003;228(1):112–8. [PubMed: 12808127]
27. Kumar G, Goldberg SN, Gourevitch S, Levchenko T, Torchilin V, Galun E, et al. Targeting STAT3 to Suppress Systemic Pro-Oncogenic Effects from Hepatic Radiofrequency Ablation. Radiology. 2017:162943.
28. Semenza GL. Hypoxia-inducible factor 1 (HIF-1) pathway. Science's STKE : signal transduction knowledge environment. 2007;2007(407):cm8.
29. Calderwood SK. Heat shock proteins and cancer: intracellular chaperones or extracellular signaling ligands? Philos Trans R Soc Lond B Biol Sci. 2018;373(1738).
30. Lang BJ, Nguyen L, Nguyen HC, Vieusseux JL, Chai RC, Christophi C, et al. Heat stress induces epithelial plasticity and cell migration independent of heat shock factor 1. Cell Stress Chaperones. 2012;17(6):765–78. [PubMed: 22791010]
31. Bulvik B, Rozenblum N, Gourevitch S, Ahmed M, Galun E, Goldberg SN. IRE versus RFA: A comparison of local and systemic effects in a small animal model. Radiology. 2015;[in press].
32. Faroja M, Ahmed M, Appelbaum L, Ben-David E, Moussa M, Sosna J, et al. Irreversible electroporation ablation: is all the damage nonthermal? Radiology. 2013;266(2):462–70. [PubMed: 23169795]
33. Moussa M, Goldberg SN, Kumar G, Sawant RR, Levchenko T, Torchilin VP, et al. Nanodrug-enhanced radiofrequency tumor ablation: effect of micellar or liposomal carrier on drug delivery and treatment efficacy. PLoS One. 2014;9(8):e102727. [PubMed: 25133740]

34. Poulou LS, Botsa E, Thanou I, Ziakas PD, Thanos L. Percutaneous microwave ablation vs radiofrequency ablation in the treatment of hepatocellular carcinoma. World J Hepatol. 2015;7(8): 1054–63. [PubMed: 26052394]

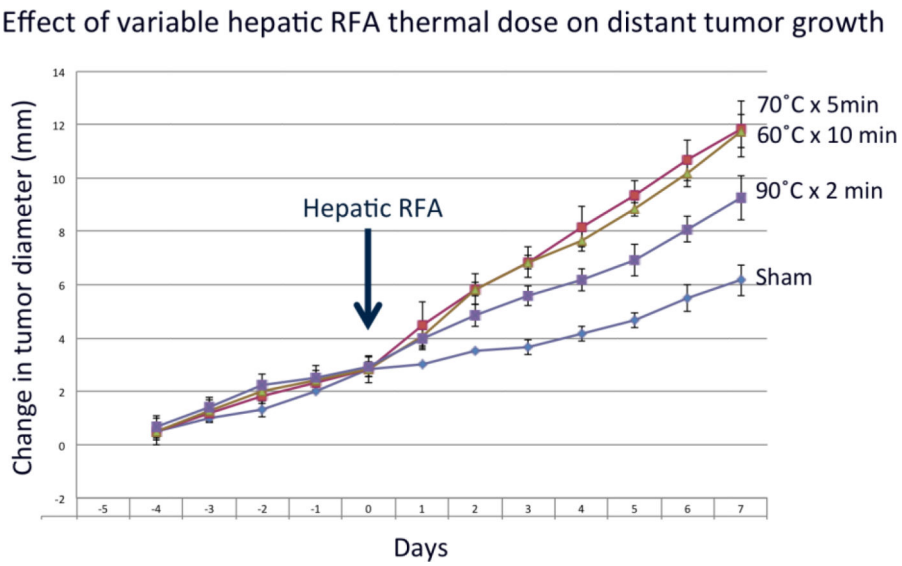

Figure 1. RFA thermal dose settings during hepatic ablation stimulate variable distant subcutaneous tumor growth.

Animals implanted with subcutaneous R3230 tumors were treated with low- (60°Cx10min), medium- (70°Cx5min) and high-dose (90°Cx2min) hepatic RF ablation compared to sham treatment. After hepatic ablation (Day 0), the growth rates of the distant tumors significantly increased for low- and medium-dose RFA compared to high-dose RFA and sham treatment. This resulted in significantly larger tumor size ($p<0.05$) at day 7 for low- and medium-dose RFA compared high-dose RFA and sham treatment. A significant increase in tumor growth was still seen in high-dose RFA compared to sham ($p<0.05$), however the effect is much less pronounced.

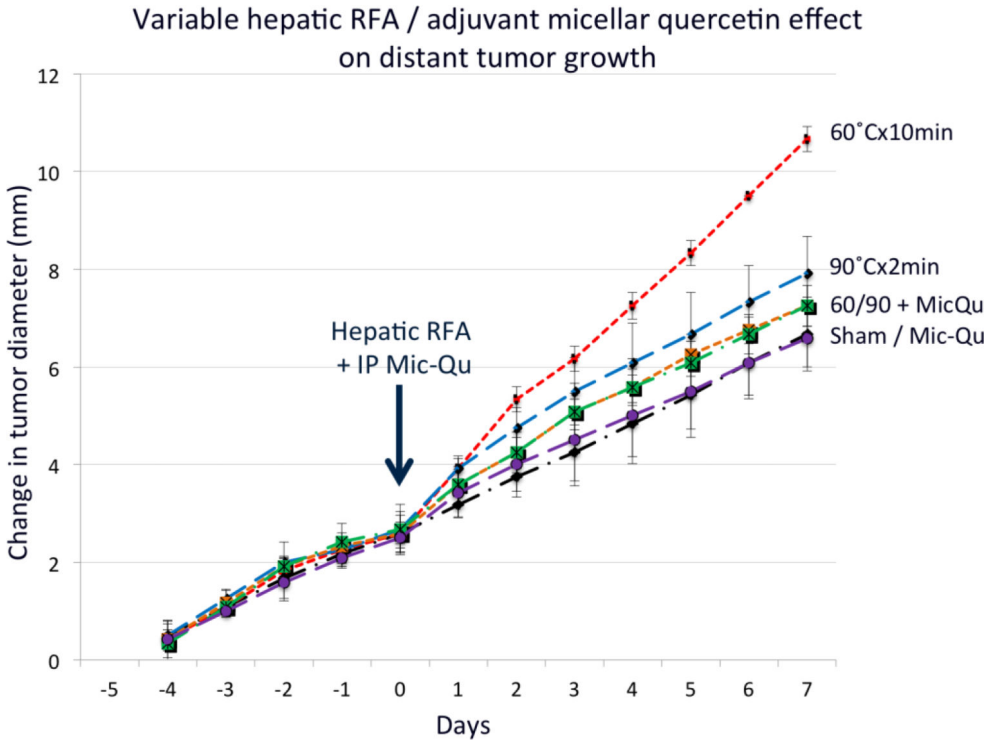

Figure 2. Adjuvant micellar quercetin administered at the time of hepatic RFA suppresses distant subcutaneous tumor growth.

Animals implanted with subcutaneous R3230 tumors were treated with low-dose (60°Cx10min) and high-dose (60°Cx10min) hepatic RFA with and without single-dose micellar quercetin (Mic-Qu) compared to sham treatment and micellar quercetin alone (total 6 treatment arms). After hepatic ablation (Day 0), the growth rates of the distant R3230 tumors significantly increased for low-dose RFA and to a lesser degree, high-dose RFA compared to sham treatment. Adjuvant micellar quercetin significantly reduced distant tumor growth rates of both doses down to near-baseline levels ($p<0.01$ for all comparisons).

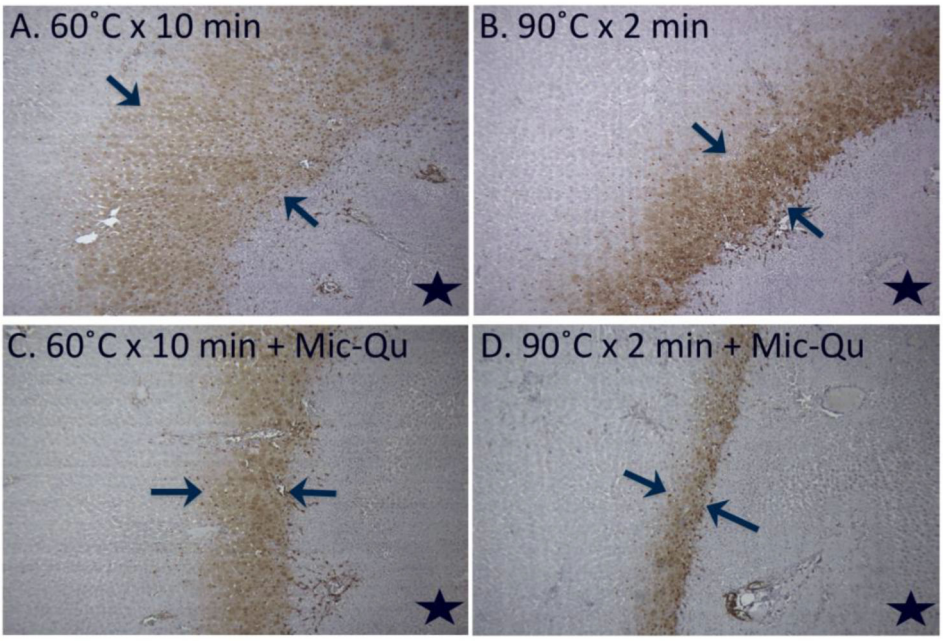

Figure 3. Adjuvant micellar quercetin suppresses HSP expression in the periablational rim.
Marked hepatic ablation-induced HSP70 expression (bracketed by arrows in all images) after (A) low-dose (60°Cx10min) and (B) high-dose (90°Cx2min) ablation is significantly reduced with adjuvant single-dose micellar quercetin administered at the time of ablation (Day 0) for both (C) low- and (D) high-dose RFA ($p<0.01$ for all comparisons). The black star denotes the ablation zone.

Table 1.

Summary of subcutaneous tumor growth and proliferative index for different hepatic RF ablation parameters without and with adjuvant micellar quercetin.

A detailed summary of tumor growth data (including pre- and post-treatment tumor measurements growth curve slopes) is provided. Immunohistochemistry quantification of proliferative index (Ki-67 % cell positivity) is also provided. Statistically significant differences (defined as $p<0.05$) are annotated.

Treatment arms	End Diameter at 7d (mm)	Pre Growth Curve Slope	Post Growth Curve Slope	Ki-67 % cell positivity	Microvascular density (#/hpf)
Hepatic RF ablation in animals with subcutaneous R3230 tumors					
Sham	13.5±0.5	0.54±0.03	0.47±0.06	29.2±1.2	13.8±0.3
Low (60°C x 10 min)	18.1±0.4 *	0.59±0.09	1.22±0.13 *	58.4±1.0 *	22.8±3.1 *
Medium (70°C x 5 min)	19.2±0.8 *	0.58±0.09	1.26±0.07 *	63.6±4.3 *	44.2±0.3 *
High (90°C x 2 min)	16.4±0.7 *	0.60±0.09	0.85±0.08 *	43.6±1.6 *	16.7±1.5 *
Hepatic RFA with adjuvant micellar quercetin in animals with subcutaneous R3230 tumors					
Sham / MQ	14.1±0.6	1.01±0.23 **	0.76±0.15	31.8±0.9	13.2±1.5
Low (60°C x 10 min) / MQ	14.6±0.4 ¥	1.01±0.23	1.13±0.29 *	39.4±1.8 ¥	13.4±1.6 ¥
High (90°C x 2 min) / MQ	14.6±0.5 ¥	1.01±0.23	0.56±0.08	40.0±1.3	13.7±1.3

* $p<0.05$ when compared to sham group

** pre-treatment growth rates same for each MQ arm

¥ $p<0.05$ when compared to corresponding RFA alone arms in two-tailed T-test

Table 2.

Summary of changes in serum, liver, and distant tumor HGF and VEGF levels for variable hepatic RF ablation without and with adjuvant micellar quercetin therapies.

	IL-6 at 6h (pg/ml)		HGF at 72h (pg/ml)		VEGF at 72h (pg/ml)
Treatment	**Liver**	**Serum**	**Liver**	**Serum**	**Liver**
Sham	2,189 ± 106	264 ± 7	21,758 ± 961	2,851 ± 208	7,536 ± 127
Low / 60°Cx10min	2,956 ± 265 *	452 ± 8 *	33,619 ± 1110 *	3,987 ± 47 *	13,036 ± 1214 *
High / 90°C x2min	2,486 ± 72 *	348 ±17 *	25,453 ± 752 *	3,537 ± 202 *	8,925 ± 464 *
Treatment with adjuvant micellar quercetin					
Sham / MQ	2,167 ± 134	262 ± 9	22,175 ± 220	2,884 ± 317	7,703 ± 293
Low / 60°Cx10min / MQ	2,903 ± 108 *	442 ±18 *	22,092 ± 507 ¥	2,756 ± 276 ¥	9,528 ± 821 ¥
High / 90°C x2min / MQ	2,503 ± 60 *	359 ±19 *	21,897 ± 1329 ¥	2,554 ± 225 ¥	8,036 ± 699

* p<0.05 when compared to sham group

** pre-treatment growth rates same for each MQ arm

¥ p<0.05 when compared to corresponding RFA alone arms in two-tailed T-test